Draft Version June 27, 2017
Preprint typeset using LaTeX style emulateapj v. 12/16/11

PLANCK CLUSTER PAPER

SB[1], JPH[1], FM

Draft Version June 27, 2017

ABSTRACT

We propose to continue our program of optical imaging to unveil all of the most massive clusters in the observable Universe. We start from the all-sky Planck Sunyaev-Zeldovich (SZ) catalogs, which contain several hundred high significance (signal-to-noise ratio, SNR > 5) unconfirmed cluster candidates. Since SZ selection favors high mass clusters and the Planck confirmation process favored low redshift systems, the highest significance unconfirmed candidates are, therefore, likely massive clusters ($M_{500} > 5 \times 10^{14}$ $M_\odot$) at relatively high redshift ($z > 0.5$). Our proposed observations, using MOSAIC-3 on Mayall, are designed to confirm the presence of a brightest cluster galaxy (to $z \sim 1$) and red sequence of accompanying cluster members (to $z \sim 0.7$). Preliminary results from our observations over the past two years have validated our approach by the detection of optical clusters in a number of Planck candidates, including the discovery of rich systems at $z = 0.553$ and $z = 0.830$ that rival the most massive clusters known. The proposed observations represent the first step required to provide a complete all-sky census throughout the observable Universe of the most massive, high redshift clusters. Their expected high redshift and high mass make the unconfirmed Planck clusters, arguably, the most important available sample for probing deviations from ΛCDM and defining the high-mass end of the cluster mass function.

Subject headings:

1. INTRODUCTION

this section has not been edited and is just a bunch of stuff copy and pasted. I did update some of the references. Massive galaxy clusters at high redshifts are rare beasts that hold important clues to the evolution of structure in the Universe and in principle can help probe (or falsify) structure formation models under the ΛCDM paradigm (e.g., Mortonson et al. 2011; Harrison & Coles 2012; Harrison & Hotchkiss 2012; Waizmann et al. 2012; Zitrin et al. 2009). Galaxy clusters also harbor a significant fraction of the visible baryons in the Universe, in the form of a hot intracluster medium that leaves an imprint on the Cosmic Microwave Background (CMB) though the Sunyaev-Zel'dovich (SZ; Sunyaev & Zeldovich 1972 effect.

The surface brightness of the SZ effect does not depend on redshift, therefore providing uniform samples of massive clusters up to arbitrary distances. This has been borne out by the large area surveys of the Atacama Cosmology Telescope (ACT; Swetz et al. 2011) and the South Pole Telescope (SPT; Carlstrom et al. 2011 that have detected hundreds of massive clusters since 2008 up to redshifts of $z \sim 1.4$ (see Reichardt et al. 2013 and Hasselfield et al. 2013 for latest results). Now, Planck has released an all-sky SZ sample (PSZ; Planck Collaboration et al. 2014) that contains 861 confirmed clusters (of which most [683] were known previously) and another 366 unconfirmed cluster candidates.

We led the ACT cluster confirmation process using 4-m class telescopes; now we propose to use our well-established expertise to identify Planck clusters. The recent SZ cluster samples have opened a new window into extreme systems, the most massive clusters at high redshift (Foley et al. 2011; Menanteau et al. 2012), prompting studies that match their observed numbers with the abundance predictions of ΛCDM cosmology (Hoyle et al. 2011, Mortonson et al. 2011, Waizmann et al. 2012). There are few, if any, clusters at high redshift ($z > 0.8$) and high mass ($M_{200} > 10^{15}$ $M_\odot$) in the cosmological simulations (see Tinker et al. 2008), so the halo mass function at high-z and high-M is essentially unconstrained. Thus, with the proposed observations we will determine the abundance of massive clusters at high redshift making a direct observational measurement of the high-z, high-M end of the halo mass function. For example, one of the most impressive results of the ACT SZ survey is our discovery of the high redshift ($z = 0.87$), extreme cluster "El Gordo" (ACT-CL J0102-4915), the most significant SZ detection of the whole survey (and also of the SPT survey). Our recent HST weak-lensing analysis has provided an independent mass estimation $M_{200a} = (3.1 \pm 0.7) \times 10^{15}$ $M_\odot$ (Jee et al. 2013) that confirms our earlier mass estimates for the cluster (Menanteau et al. 2012). Based on its estimated mass alone, "El Gordo" is a very rare system within the ACT+SPT (2800 sq. deg.) survey area, but is still consistent with the expectations of ΛCDM. We are now at a unique moment in cluster science where we can discover all massive clusters in the observable universe. This census will measure the high-mass, high-redshift cluster mass function, and determine the extent of deviations from the theoretical halo mass function (Jenkins et al. 2001; Tinker et al. 2008).

Assuming WMAP7 cosmology (Komatsu et al. 2011) with the Tinker et al. (2008) halo mass function, there should be only $\sim$ 4 clusters as massive as El Gordo ($\leq 2 \times 10^{15}$ $M_\odot$) at $z > 0.6$ in the full area covered by the Planck PSZ catalog (83.7% of the sky). Although Plancks larger beam size (compared to both ACT and SPT) makes it more sensitive to clusters at lower red-

[1] Rutgers;boada@physics.tamu.edu

shifts (due to their larger projected area on the sky), among the 861 confirmed clusters in the recently released all-sky Planck SZ catalog are the two highest significance high-redshift SZ detections from ACT (as well as several other ACT and SPT clusters). This confirms the ability of Planck to unambiguously detect the most massive clusters at high redshift. In fact Planck reports "El Gordo" ($z = 0.87$) and ACT-CL J2327.40204 ($z = 0.701$) at S/N values of 8.0 and 6.3, respectively. And as Figure 2 (right panel) shows, these are the two most massive Planck clusters in the confirmed sample at high redshift. For the new clusters we confirm, our experimental design allows us to estimate photometric redshifts, which will be sufficiently accurate for a meaningful estimate of the clusters mass from the Planck SZ signal.

Unless otherwise noted, throughout this paper, we use a concordance cosmological model ($\Omega_\Lambda = 0.7$, $\Omega_m = 0.3$, and $H_0 = 70$ km s^{-1}Mpc^{-1}), assume a Chabrier initial mass function (Chabrier 2003), and use AB magnitudes (Oke 1974).

2. DESIGN

Among the recently released, second, all-sky PSZ catalog (Planck Collaboration et al. 2016) there are 366 unconfirmed SZ detections with S/N > 4.5. The vast majority of these must lie at high-z because the Planck confirmation process mostly relied on existing catalogs with a preference for low-z clusters. Furthermore, the confirmed sample has a small fraction (3%) of $z > 0.6$ clusters compared to that expected ($\sim 20\%$) based on the theoretical halo mass function (Jenkins et al. 2001; Tinker et al. 2008). If other clusters like "El Gordo" exist, they are hiding as high-significance candidates within the objects in this catalog. The design of the observations is to use both optical and near-infrared (NIR) imaging to confirm the SZ detections as real clusters and provide photometric redshifts using the multi-color information.

Our strategy is to use the Kitt Peak National Observatory (KPNO) Mayall-4m telescope imaging as the first and fundamental step to confirm the highest significance detections in the PSZ catalog that are visible across the entire northern sky. Following closely the procedure used for ACT follow-up citation?, targets are prioritized by SZ signal-to-noise (S/N). We choose to initially report on targets with PSZ S/N> 5 as the statistical reliability of PSZ cluster candidates is quite high: according to the Planck team $\sim 90\%$ of candidates at S/N> 5 turn out to be "real" clusters (citation? maybe show the figure from the proposal).

Optical imaging will be sufficient to confirm nearly all of the candidates, but for the highest redshift ones, NIR data will be necessary. Again following the procedure for ACT cluster follow-up: those candidates with some evidence for a high-z brightest cluster galaxy (BCG; note that we can detect BCGs to $z \sim 1.5$) will be targeted with NIR observations to confirm the presence of a BCG and detect the red sequence of cluster members. Observational priority again is given to higher S/N candidates.

2.1. *Observations*

All observations were conducted with the KPNO Mayall telescope. The optical observations were made with the MOSAIC camera mounted at the prime focus. Two detector packages were used for the observations. The earlier MOSAIC1.1 instrument consisted of eight 2048×4096 SITe CCDs, arranged 2×4, separated by a ~ 50 pixels gap with a pixel scale of 0.″26 pixel^{-1}. MOSAIC1.1 was replaced with Mosaic3, in year?, and consists of four new 4k×4k, 15 micron pixel, 500-micron thick LBNL deep-depletion CCDs. Because the only change from MOSAIC1.1 to MOSAIC3 are the CCDs and controllers the both versions have a $36' \times 36'$ field-of-view.

The near-IR observations utilized the National Optical Astronomy Observatory (NOAO) Extremely Wide-Field Infrared Imager (NEWFIRM; Probst et al. 2004). The instrument consists of four InSb 2048×2048 pixel arrays arranged in 2×2 with approximately $1'$ gaps between each of the CCDs. The detector has a plate scale of 0.″4 pixel^{-1} and a $28' \times 28'$ field-of-view.

need to talk about the dithering

The optical observing strategy consists of targeted *griz* observations of individual candidates with exposure times of 350 s, 350 s, 1100 s and 1100 s (assuming dark conditions) to provide 5σ detections limits of $g =$??, $r = 24.5$, $i = 24.5$, $z = 24.2$ ensuring the unambiguous detection of the faint (i.e., 0.4L$\star$) galaxies in the red cluster sequence up to $z \sim 1.0$ (citation?) and of brightest cluster galaxies (BCGs) to higher redshifts. The choice of filters in our program is driven by the need to segregate early-type galaxies in the cluster through their colors (or photometric redshifts) by sampling blueward and red-ward of the 4000Å break.

For the NEWFIRM observations, we obtained 3600 s of Ks band imaging using 60 s exposures (5 coadded 12 s exposures) taken at 60 different dither positions distributed quasi-randomly over a square $100'' \times 100''$ region. This produced reduced images with uniform exposure and sky level. The final dithered images cover approximately $28' \times 28'$ which comfortably matches the MOSAIC observations.

A NEWFIRM integration of 3600 s allows us to reach a limiting Ks magnitude of ~ 22.0 (AB, 3σ). This magnitude limit corresponds to $\sim M_\star + 2$ in the cluster luminosity function at $z = 1.0$ as measured by De Propris et al. (1999), and assuming Ks AB = Ks Vega +1.86. This surface brightness limit corresponds to $\sim M_\star + 1.0$ at $z = 1.5$, sufficient for detecting sub L$_\star$ at this limit, allowing for confident detection of the BCG and associated red cluster sequence.

TABLE 1 Basic properties of the galaxy clusters candidates targeted for observation with the MOSAIC and NEWFIRM instruments: Column 1: Cluster name; Column 2: The right ascension of the cluster; Column 3: The declination of the cluster; Column 4: the PSZ catalog S/N ratio; Column 5: The date of MOSAIC observations; Column 6: The data of NEWFIRM observations.

Cluster (1)	RA (J2000) (2)	DEC (J2000) (3)	PSZ2 SNR (4)	MOSAIC Obs. (5)	NEWFIRM Obs. (6)
PSZ2_G124.11+25.02	2:40:03	+87:38:38.73	5.5289	–	Nov, 2016

TABLE 1 Continued

Cluster (1)	RA (J2000) (2)	DEC (J2000) (3)	PSZ2 SNR (4)	MOSAIC Obs. (5)	NEWFIRM Obs. (6)
PSZ2_G125.55+32.72	11:25:35	+83:57:29.12	6.4852	Nov, 2016	Feb, 2016
PSZ2_G127.35-10.69	1:19:42	+51:56:15.39	6.941	Oct, 2014	Nov, 2014
PSZ2_G128.15-24.71	1:15:30	+37:54:48.45	4.7484	–	Nov, 2016
PSZ2_G131.27-25.82	1:28:49	+36:26:41.01	4.5022	–	Nov, 2016
PSZ2_G136.31+54.67	11:47:50	+60:45:56.07	6.9194	Jun, 2017	Feb, 2016
PSZ2_G137.24+53.93	11:41:07	+61:11:39.02	7.8731	Nov, 2016	Feb, 2016
PSZ2_G137.58+53.88	11:39:27	+61:09:01.04	8.179	Feb, 2014	Mar, 2014
PSZ2_G139.72-17.13	2:19:55	+42:49:53.97	5.1164	–	Nov, 2016
PSZ2_G144.84-35.16	2:09:42	+24:21:19.56	4.8356	–	Nov, 2016
PSZ2_G145.25+50.84	10:53:26	+60:51:43.24	5.9848	–	Feb, 2016
PSZ2_G146.88+17.13	5:34:10	+65:43:14.28	6.1331	Nov, 2016	Feb, 2016
PSZ2_G153.56+36.82	8:44:32	+62:24:41.96	15.8967	Nov, 2016	Nov, 2015
PSZ2_G153.68+36.96	8:45:33	+62:17:12.13	5.0674	Nov, 2016	Nov, 2015
PSZ2_G163.22-26.48	3:28:29	+23:50:15.15	6.3463	Nov, 2016	Feb, 2016
PSZ2_G165.39+09.22	5:47:59	+46:08:39.24	5.5998	Nov, 2016	Nov, 2016
PSZ2_G166.27-24.71	3:42:39	+23:24:41.39	9.5753	Nov, 2016	Nov, 2015
PSZ2_G166.27-25.02	3:41:44	+23:11:00.45	8.0897	Nov, 2016	Nov, 2016
PSZ2_G166.56-17.69	4:04:47	+28:21:38.16	4.7632	–	Nov, 2016
PSZ2_G167.44-38.06	3:09:12	+12:37:11.49	7.657	Oct, 2014	–
PSZ2_G171.79-42.08	3:08:40	+07:24:32.96	5.842	Nov, 2016	Feb, 2016
PSZ2_G173.76+22.92	7:17:28	+44:03:27.62	5.8035	Nov, 2016	Feb, 2016
PSZ2_G181.88-30.77	4:04:21	+09:16:14.87	9.2935	Nov, 2016	Nov, 2015
PSZ2_G183.92+16.36	7:01:57	+32:51:35.39	4.974	–	Nov, 2016
PSZ2_G185.45-32.01	4:08:04	+06:06:33.99	4.992	Jan, 2014	Nov, 2014
PSZ2_G189.79-37.25	3:59:37	+00:07:54.80	7.278	Oct, 2014	Nov, 2014
PSZ2_G191.82-26.64	4:38:37	+04:42:02.64	6.172	Nov, 2016	Feb, 2016
PSZ2_G192.40-67.89	2:18:20	-17:45:23	7.0301	Nov, 2016	Feb, 2017
PSZ2_G194.68-49.76	3:25:22	-9:40:50	5.712	Nov, 2016	Nov, 2016
PSZ2_G210.37-37.00	4:32:44	-14:03:01	9.8447	Nov, 2016	Nov, 2015
PSZ2_G210.71+63.08	10:51:42	+24:58:09.19	7.3734	Jun, 2017	Feb, 2016
PSZ2_G210.78-36.25	4:36:07	-14:02:58	6.3181	Nov, 2016	Feb, 2016
PSZ2_G216.25+10.10	7:33:26	+01:40:36.28	5.518	–	Nov, 2016
PSZ2_G228.35-66.31	2:38:41	-30:50:21	9.0827	–	Nov, 2016
PSZ2_G230.28-28.57	5:31:09	-26:49:29	9.3019	–	Nov, 2016
PSZ2_G235.96+38.21	9:46:11	+00:29:10.03	9.396	–	Feb, 2016
PSZ2_G237.68+57.83	10:53:31	+10:48:56.98	5.3631	–	Jan, 2017
PSZ2_G246.86-12.29	7:08:10	-35:37:39	7.862	–	Dec, 2014
PSZ2_G252.45+73.44	11:58:35	+16:00:18.38	5.5683	–	Feb, 2016
PSZ2_G253.44-10.93	7:28:33	-40:51:17	7.075	–	Dec, 2014
PSZ2_G254.52+62.52	11:29:57	+07:35:04.97	4.8476	–	Jan, 2017
PSZ2_G270.88+37.23	11:05:19	-18:56:55	5.4886	–	Jan, 2017
PSZ2_G305.76+44.79	12:59:54	-18:01:59	5.717	–	Feb, 2016
PSZ2_G310.81+83.91	12:55:01	+21:05:41.16	8.2891	Nov, 2016	Feb, 2016
PSZ2_G318.46+83.79	12:58:33	+21:08:11.93	9.401	Feb, 2014	Mar, 2014
PSZ2_G320.94+83.69	12:59:47	+21:06:56.63	7.3218	Jun, 2017	Feb, 2016
PSZ2_G328.96+71.97	13:23:13	+10:43:41.59	5.8516	Jun, 2017	Feb, 2016

A summary of our observations is given in Table 1.

3. DATA REDUCTION AND CALIBRATION

Standard image reductions including subtraction of dark frames, flat fielding, sky-subtraction, and bad pixel masking was performed by the NOAO virtual observatory using the MOSAIC (Valdes & Swaters 2007) and NEWFIRM (Swaters et al. 2009) science pipelines. The resultant FITS files consist of fully reduced images with either all single exposure CCDs mosaicked into a single image extension (as in the case of Mosaic1.1 and NEWFIRM) or as a multi-extension FITS file with each single exposure CCD occupying a separate extension.

We then mosaic each separate exposure into a master mosaic as described in the following section.

3.1. *Mosaicking*

Combined mosaics are created with SWARP (Bertin et al. 2002). The individual dither frames are stacked and then median combined to produce the final completed mosaic. The final mosaic retains the native plate scale, and header information. The final exposure time is calculated as the median exposure time of the combined images, and similarly the final airmass is median of the individual air masses. need to talk about the weight images

The full parameter file used while creating the mosaics is given in Appendix A.

3.2. *Astrometric Calibration*

Each of the final mosaics produced in the previous section are first astrometrically aligned with *Gaia* (Gaia Collaboration et al. 2016a) Data Release 1 (Gaia Collaboration et al. 2016b) using SCAMP (Bertin 2006) as a part of PHOTOMETRYPIPELINE (PP; Mommert & M. 2017).

Sources are extracted from the mosaics with a signal-to-noise ratio (SNR) of at least ten and with a minimum area of at least 12 pixels. The extracted sources are then matched to the *Gaia* data and a new astrometric solution is calculated. Because the initial astrometric solution from the VO is quite accurate, the resultant corrections are less than 1″.

3.3. *Photometric Calibration*

After the mosaics have been astrometrically aligned, we use PP to produce a photometric solution. PP calculates a photometric zero-point in each of our observed bands by comparing field stars located throughout the mosaic to known photometry from large-area sky surveys. Because our sources are spread across the entire northern sky, and because we prefer to minimize the number of differences between photometric solutions we are limited to two surveys. We first seek photometric data from the *Sloan Digital Sky Survey* (SDSS; York et al. 2000) Data Release 13 (Alam et al. 2015) get a new citation for dr13 this is for dr12. When our target does not lie within the SDSS footprint we utilize the Panoramic Survey Telescope and Rapid Response System (Pan-STARRS; Chambers et al. 2016) Data Release 1 (hereafter PS1; Flewelling et al. 2016). Both surveys provide accurate *griz* magnitudes and large on-line queriable databases for rapid automated calibration.

Sources are extracted from the combined mosaics with a $3''$ diameter aperture; sources with a SNR$\geq$ 10 are matched to a survey catalog and a photometric zero-point is determined. We use half of the available stars (with accurate catalog photometry) to derive the zero-point resulting in zero-points calculated from approximately $10-500$ stars and with typical uncertainties of give zp errors in the different bands.

Should we talk about the difference between us and SDSS? If so, how should we "sum up" the differences in a simple way?

4. ANALYSIS

lorem

4.1. *Source Extraction and Photometry*

For source extraction and photometry estimation we use Source Extractor (hereafter SExtractor; Bertin & Arnouts 1996) run dual image mode where the i image serves as a detection image. See Appendix B for a complete parameter listing. Science catalog photometry is compared to the

4.2. *Photometric Redshifts*

We determine photometric redshifts (photo-z) from the four-band optical images using Bayesian Photometric Redshifts (BPZ; Benitez 2000; Coe et al. 2006) following the same procedure as in Menanteau et al. (2008).

We assess the effectiveness of our photo-z estimates by comparing with the available spectroscopic redshifts (spec-z) from the SDSS. We use three diagnostics to gauge photo-z accuracy. First, we report the full scatter between the photo-z and spec-z, defined as:

$$\sigma_f = \mathrm{RMS}[\delta z/(1+z_{spec})] \tag{1}$$

where $\delta z = z_{spec} - z_{phot}$. Second, we report the normalized median absolute deviation (NMAD; Ilbert et al. 2009; Dahlen et al. 2013; Molino et al. 2017), given as

$$\sigma_{NMAD} = 1.48 \times \mathrm{median}\left(\frac{|\delta z|}{1+z_{spec}}\right). \tag{2}$$

which provides an estimate of the scatter resistant to catastrophic outliers. Finally, the catastrophic outlier fraction (OLF) where we define a catastrophic outlier (following Molino et al. 2017) as,

$$\eta = \frac{|\delta z|}{(1+z_{spec})} > 5 \times \sigma_{NMAD}. \tag{3}$$

4.3. *Cluster Finding*

We create RGB images using STIFF (Bertin & Emmanuel 2011). We use MaxBCG (Koester et al. 2007).

5. RESULTS AND DISCUSSION

lorem

6. SUMMARY

lorem

ACKNOWLEDGEMENTS

This research made use of APLpy, an open-source plotting package for Python hosted at http://aplpy.github.com; the IPython package (Perez & Granger 2007); MATPLOTLIB, a Python library for publication quality graphics (Hunter 2007). IRAF is distributed by the National Optical Astronomy Observatory, which is operated by the Association of Universities for Research in Astronomy under cooperative agreement with the National Science Foundation (Tody 1993). PyRAF is a product of the Space Telescope Science Institute, which is operated by AURA for NASA. Funding for the SDSS and SDSS-II has been provided by the Alfred P. Sloan Foundation, the Participating Institutions, the National Science Foundation, the U.S. Department of Energy, the National Aeronautics and Space Administration, the Japanese Monbukagakusho, the Max Planck Society, and the Higher Education Funding Council for England. The SDSS Web Site is http://www.sdss.org/. The SDSS is managed by the Astrophysical Research Consortium for the Participating Institutions. This work has made use of data from the European Space Agency (ESA) mission *Gaia* (https://www.cosmos.esa.int/gaia), processed by the *Gaia* Data Processing and Analysis Consortium (DPAC, https://www.cosmos.esa.int/web/gaia/dpac/consortium). Funding for the DPAC has been provided by national institutions, in particular the institutions participating in the *Gaia* Multilateral Agreement.

REFERENCES

Alam, S., Albareti, F. D., Prieto, C. A., et al. 2015, The Astrophysical Journal Supplement Series, 219, 12
Benitez, N. 2000, The Astrophysical Journal, 536, 571
Bertin, E. 2006, in Astronomical Society of the Pacific Conference Series, Vol. 351, Astronomical Data Analysis Software and Systems XV, ed. C. Gabriel, C. Arviset, D. Ponz, & S. Enrique, 112
Bertin, E., & Arnouts, S. 1996, Astronomy and Astrophysics Supplement Series, 117, 393
Bertin, E., & Emmanuel. 2011, Astrophysics Source Code Library, record ascl:1110.006

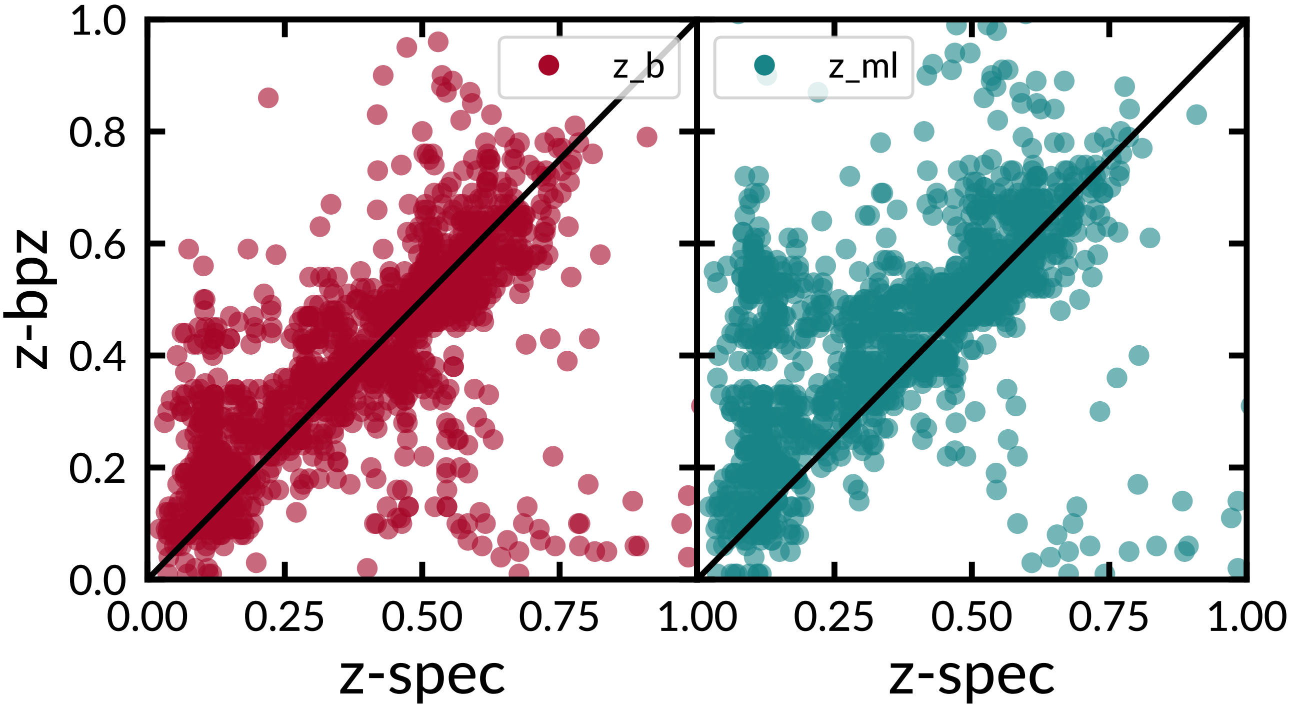

FIG. 1.— This is a placeholder figure for a figure about how we are doing with the photo-z's. I'm still working out exactly what we should show on the figure, and whether it should be a single or double column figure.

Bertin, E., Mellier, Y., Radovich, M., et al. 2002, in Astronomical Society of the Pacific Conference Series, Vol. 281, Astronomical Data Analysis Software and Systems XI, ed. D. Bohlender, D. Durand, & T. Handley, 228

Carlstrom, J. E., Ade, P. A. R., Aird, K. A., et al. 2011, Publications of the Astronomical Society of the Pacific, 123, 568

Chabrier, G. 2003, Publications of the Astronomical Society of the Pacific, 115, 763

Chambers, K. C., Magnier, E. A., Metcalfe, N., et al. 2016, eprint arXiv:1612.05560, arXiv:1612.05560

Coe, D., Benitez, N., Sanchez, S. F., et al. 2006, The Astronomical Journal, 132, 926

Dahlen, T., Mobasher, B., Faber, S. M., et al. 2013, The Astrophysical Journal, 775, 93

De Propris, R., Stanford, S. A., Eisenhardt, P. R., Dickinson, M. E., & Elston, R. 1999, The Astronomical Journal, Volume 118, Issue 2, pp. 719-729., 118, 719

Flewelling, H. A., Magnier, E. A., Chambers, K. C., et al. 2016, eprint arXiv:1612.05243, arXiv:1612.05243

Foley, R. J., Andersson, K., Bazin, G., et al. 2011, The Astrophysical Journal, 731, 86

Gaia Collaboration, G., Brown, A. G. A., Vallenari, A., et al. 2016a, Astronomy & Astrophysics, Volume 595, id.A2, 23 pp., 595, arXiv:1609.04172

Gaia Collaboration, G., Prusti, T., de Bruijne, J. H. J., et al. 2016b, Astronomy & Astrophysics, Volume 595, id.A1, 36 pp., 595, arXiv:1609.04153

Hunter, J. D. 2007, Computing in Science & Engineering, 9, 90

Ilbert, O., Capak, P., Salvato, M., et al. 2009, The Astrophysical Journal, 690, 1236

Jenkins, A., Frenk, C. S., White, S. D. M., et al. 2001, Monthly Notices of the Royal Astronomical Society, 321, 372

Koester, B. P., McKay, T. A., Annis, J., et al. 2007, The Astrophysical Journal, 660, 221

Komatsu, E., Smith, K. M., Dunkley, J., et al. 2011, The Astrophysical Journal Supplement Series, 192, 18

Menanteau, F., Hughes, J. P., Jimenez, R., et al. 2008, The Astrophysical Journal, Volume 698, Issue 2, pp. 1221-1231 (2009)., 698, 1221

Menanteau, F., Hughes, J. P., Sif?n, C., et al. 2012, The Astrophysical Journal, 748, 7

Molino, A., Benítez, N., Ascaso, B., et al. 2017, eprint arXiv:1705.02265, arXiv:1705.02265

Mommert, M., & M. 2017, Astronomy and Computing, 18, 47

Oke, J. B. 1974, The Astrophysical Journal Supplement Series, 27, 21

Perez, F., & Granger, B. E. 2007, Computing in Science & Engineering, 9, 21

Planck Collaboration, Ade, P. A. R., Aghanim, N., et al. 2014, Astronomy & Astrophysics, 571, A29

—. 2016, Astronomy & Astrophysics, 594, A27

Probst, R. G., Gaughan, N., Abraham, M., et al. 2004, in Ground-based Instrumentation for Astronomy. Edited by Alan F. M. Moorwood and Iye Masanori. Proceedings of the SPIE, Volume 5492, pp. 1716-1724 (2004)., Vol. 5492, 1716

Sunyaev, R. A., & Zeldovich, Y. B. 1972, Comments on Astrophysics and Space Physics, 4

Swaters, R., Valdes, F., & Dickinson, M. 2009, in Astronomical Society of the Pacific Conference Series, Vol. 411, Astronomical Data Analysis Software and Systems XVIII, ed. D. Bohlender, D. Durand, & P. Dowler, 506

Swetz, D. S., Ade, P. A. R., Amiri, M., et al. 2011, The Astrophysical Journal Supplement Series, 194, 41

Tinker, J., Kravtsov, A. V., Klypin, A., et al. 2008, The Astrophysical Journal, 688, 709

Tody, D. 1993, Astronomical Data Analysis Software and Systems II, 52

Valdes, F., & Swaters, R. 2007, in Astronomical Society of the Pacific Conference Series, Vol. 376, Astronomical Data Analysis Software and Systems XVI, ed. R. Shaw, F. Hill, & D. Bell, 273

York, D. G., Adelman, J., Anderson, John E., J., et al. 2000, The Astronomical Journal, 120, 1579

APPENDIX

SWARP

SEXTRACTOR